12-2007

EFFECTS OF SUPPORT GRID VANE ANGLES ON SINGLE PHASE HEAT TRANSFER WITHIN ROD BUNDLE SUBCHANNELS

Michael Cosby
Clemson University, mcosby@clemson.edu

EFFECTS OF SUPPORT GRID VANE ANGLES ON SINGLE PHASE HEAT TRANSFER WITHIN ROD BUNDLE SUBCHANNELS

A Thesis
Presented to
the Graduate School of
Clemson University

In Partial Fulfillment
of the Requirements for the Degree
Master of Science
Mechanical Engineering

---

by
Michael C. Cosby
December 2007

Accepted by:
Dr. Donald E. Beasley, Committee Chair
Dr. Richard S. Figliola
Dr. Richard S. Miller

ABSTRACT

The main goal of this project is to investigate how changes in support grid mixing vane angles affect the single phase heat transfer coefficient for rod bundle flows. Since other studies have been done on these types of flows, the present study also serves the purpose of further solidifying conclusions made in those works. A split-pair mixing vane support grid without weld nugget cutouts is thought to have optimum flow characteristics at a vane angle of 29 degrees. Results obtained from this work have shown this to be true.

Vane angles were modified to angles of 37 °, 33° and 21° using a custom designed tool and visually inspected using gauge blocks. Data was also taken at the original angle of 29° as a baseline. Temperature measurements were directly obtained from the rod surface using a sensor comprised of 4 E-type thermocouples. Because of the known behavior of rod bundle subchannel flows, temperature measurements were taken between -5 and 40 hydraulic diameters with respect to the support grid's trailing edge. At each axial location, the sensor was rotated at 22.5° increments for a total of 16 angular measurement positions at the inner surface of the rod. Forced convection heat transfer was achieved by way of direct resistance heating of the rods and a high speed, pressure driven air flow. The maximum flow rate available is utilized for each test but ranged from 24,000 to 30,000 (Re) because of ambient air temperature variations. For repeatability purposes, current and voltage were set at approximately 700 amps and 4 volts respectively for each test. Results from this study along with parallel research include but are not limited to the following; circumferentially averaged Nusselt Numbers, azimuthal heat transfer variations and average turbulent kinetic energy. From a systems perspective,

any information directly pertaining to heat transfer on the fuel rod's surfaces will be helpful in the future as nuclear power becomes more prevalent. This study includes a brief introduction of the work being presented as well as a summary of past works. Along with the background information, a detailed overview of the experimental facility and method is presented. In the latter sections of this thesis, all results obtained have been thoroughly analyzed and conclusions have been made accordingly.

TABLE OF CONTENTS

Page

TITLE PAGE i

ABSTRACT ii

LIST OF FIGURES v

NOMENCLATURE vii

CHAPTER

1. INTRODUCTION 1
2. BACKGROUND 5
3. EXPERIMENTAL FACILITY 11
4. DATA ANALYSIS 24
5. RESULTS AND DISCUSSION 27
6. CONCLUSION 38

APPENDIX 40

REFERENCES 44

LIST OF FIGURES

Figure		Page
3.1	Flow Apparatus Diagram	17
3.2	Photograph of the Flow Facility	18
3.3	Rod Bundle Support Grid Locations	18
3.4	Photograph of the Assembled Rod Bundle	19
3.5	Photograph of the Test Support Grids	19
3.6	Vane Angle Tool	20
3.7	Dual Angle Gauge (37°, 33°)	20
3.8	Photograph of the Vane Angle Tool/Gauge set	21
3.9	Photograph of the Test Support Grids	21
3.10	Photograph of the Instrumented Sensor	22
3.11	Photograph of Rod Bundle w/ Copper Connection Plate	22
3.12	Photograph of Angle Gauge Installed in Support Grid	23
5.1	Center Rod Subchannel Locations	27
5.2	Lateral Velocity Field at 10 D_H	28
5.3	Split-Pair mixing Vane Pattern	29
5.4	Averaged Kinetic Energy Density @ 29°	30
5.5	Averaged Kinetic Energy Density @ 21°, 29°, 37°	31
5.6	Bulk/Surface Temperature development (vane angle 29°)	33
5.7	Heat transfer enhancement for a vane angle of 29°	34
5.8	Heat transfer enhancement for Vane Angles 37°, 33°, 29°, and 21°	34
5.9	Azimuthal Variations in Heat Transfer for a Vane Angle of 29°	36

5.10 Azimuthal Variations in Heat Transfer for a Vane Angle of 29° 36

A.1 Azimuthal Variations in Heat Transfer at 0 D_H 40

A.2 Azimuthal Variations in Heat Transfer at a Vane Angle of 37° 40

A.3 Azimuthal Variations in Heat Transfer at a Vane Angle of 33° 41

A.4 Azimuthal Variations in Heat Transfer at a Vane Angle of 29° 41

A.5 Azimuthal Variations in Heat Transfer at a Vane Angle of 21° 42

A.6 Heat transfer enhancement for Vane Angles 37°, 33°, 29°, and 21° 43

NOMENCLATURE

A_{RB}	open flow area through the rod bundle
A_{SC}	flow area through the a subchannel
A_{sp}	frontal area of the support grid
C_P	specific heat of air
D	rod diameter
D_H	hydraulic diameter of the rod bundle subchannel
HTC	heat transfer coefficient
KED	turbulent kinetic energy density
$\dot{M}$	mass flow rate
$\dot{M}_{SCFM}$	standard mass flow rate
Nu	Nusselt number
Nu_{fd}	fully developed Nusselt number
P	rod pitch
P_{RB}	wetted perimeter of the rod bundle
P_{SC}	wetted perimeter of the rod bundle
q''	heat flux
Q	electric power
Q_{ACFM}	actual volumetric flowrate
Q_{SCFM}	standard volumetric flowrate
RB_A	heated surface area of the rod bundle
Re	Reynolds number

T	temperature
T_B	bulk temperature
T_f	film temperature
T_S	surface temperature
T_s	surface temperature
U	velocity
X	axial location
Z	axial coordinate reference to support grid

Greek letters

ε_g	grid blockage ratio
ε_s	blockage ratio of support grid strap
Ø	vane angle
Θ	azimuthal location
ρ	density
μ	dynamic viscosity
ν	kinematic viscosity

CHAPTER ONE
INTRODUCTION

As fossil fuels are continually being consumed, the scientific community is concentrating it's efforts on ways to resolve the ensuing energy crisis. Since mankind has always been dependent on the combustion of fossil fuels for energy, solving this problem will not be an easy task. Power generation today is highly dependent on the combustion of coal and other fossil fuels. Not only is generating power in this way inefficient but also extremely unclean and harmful to the environment. But because of its availability and relative inexpensiveness, these coal burning plants continually dominate energy production from a global perspective. Other methods such as hydroelectric and geothermal power generation are limited for geographical reasons. It was once thought that the use of solar power would one day be used more widespread but thus far solar power has proven to be unsuitable for use on a large scale. The only existing technology that is not limited such as the aforementioned ones is nuclear power. Releasing energy at the atomic level is vastly superior to combustion or any other known chemical/mechanical processes, but for numerous reasons including safety, nuclear power generation has not been utilized to its full capabilities in the past. That being said, as the energy crisis places economic strain on the industry, nuclear power is steadily gaining ground.

At the most basic level, electricity is produced by applying shaft power to generators. This mechanical power is generated from turbines which are driven by flow and pressure. As previously stated the most common method for this is to generate steam

by using the heat from a large coal burning combustor. For nuclear power, a fission reaction inside a fuel rod bundle replaces the combustor. These types of reactors are usually referred to as pressurized water reactors. The reaction is throttled by changing the axial distance between the control rods and the fuel rods. Heat is transferred directly from the fuel rod surfaces to a high pressure water flow by the mechanism of forced convection (single phase). Obviously, one can more efficiently generate electricity by improving the single phase heat transfer coefficient. Support grids or spacers as they are sometimes called are used to keep the fuel rods positioned in a desired geometrical array such as triangular, square or hexagonal. Most commercial grade reactors have support grids designed for a 17 x 17 square array. In a study by Holloway et al. (2005), it was shown that slight changes to features on the rod bundle support grid can significantly affect the heat transfer coefficient for certain regions in the flow. Support grid features such as vanes or discs were shown to enhance the heat transfer coefficient in the range of 80% at 0 D_H and approximately 10% at 10 D_H respectively. For certain support grid geometries there was a reduction in heat transfer for certain locations below the fully developed value. This was usually on the order of 10% and only existed in a small portion of the flow where enhanced turbulent kinetic energy had decayed. The Holloway study (2005) also examined changes in the circumferential temperature variations. It was found that hot streaks developed on the rod surface depending on the amount of mixing/turbulence present in the flow.

This particular study more closely examines certain aspects of the Holloway et al. (2005) project which was sponsored by Westinghouse. The main objective of this project is to study the effects of vane angles on the single phase heat transfer coefficient. The

support grid selected for this project implements split-pair mixing vanes at an optimum vane angle of 29°. This particular grid also retains the weld nuggets. According to previous work done internally at Westinghouse, a vane angle of 29° should have the highest initial heat transfer enhancement and should also retain the swirling flow structure at increased axial distances downstream of the support grid. The current support grids will be modified for vane angles of 37°, 33° and 21°. It should also be noted that that all experimental facilities/equipment used in this project are retained from the Holloway project (2005). To prevent unrepeatable results and increased uncertainties, the only modifications made to the experimental setup will be strictly limited to those absolutely necessary such as facility maintenance and altering of the vane angles for study purposes. This project also parallels a simultaneous work by Stovall (2007), where the flow properties such as average kinetic energy density and velocity are compared for different vane angles.

The convective heat transfer coefficient will be directly determined from temperatures taken on the inside diameter of the center rod (5x5 bundle). Temperatures were taken at approximately 20 axial location and 16 angular positions. The axial data was taken at unequal intervals between support grids 2 and 3. Data was purposely taken more frequently in more chaotic areas of the flow to ensure that any abrupt changes in the temperature profile were captured. This is extremely important in the region directly downstream of the support grid's trailing edge where the swirling flow decays more rapidly. All temperature data was taken using Pdaq view software. A total of 16 temperature measurements were taken at each axial location and then averaged for increased accuracy. Using the raw data, the following results were obtained,

circumferentially averaged heat transfer coefficients with respect to axial location, Nusselt numbers and azimuthal heat transfer variations.

From this study along with comparative analysis of past works, it was found how slight changes in the vane angles affect temperature profiles and heat transfer within fuel rod bundle subchannels. More detailed background information pertaining to the experiment will be discussed in Chapter 3.

CHAPTER TWO
BACKGROUND

Several investigations of flow and heat transfer within rod bundle subchannels have been done. Past studies of these topics have lead to the development and optimization of rod bundle support grid geometry for improved heat transfer performance. The following literature survey focuses on briefly summarizing the general findings of past and current studies concerning flow and heat transfer within rod bundle subchannels. Emphasis has been placed on studies directly concerned with flow conditions, temperature profiles and heat transfer affected by rod bundle support grid features and/or geometry.

Flow conditions within rod bundle subchannels are dependent on several factors. Support grid geometry, rod pitch/diameter ratio (P/D) and total number of rods all have a tremendous effect on flow within the subchannels. Several researchers have attempted to develop correlations that would generally be valid for a large number of rod bundle configurations. Both increased mixing and higher velocities greatly enhance the single phase heat transfer coefficient and thereby increase the total amount of energy that can be extracted from the fuel rod elements. For this reason, rod bundle support grids have been designed to increase turbulence in the rod bundle subchannel. The subchannel is the open flow area between fuel rods. This turbulent effect however, only occurs in the regions close to the support grids. Further downstream the mixing, swirling flow decays and fully developed conditions are reached (boundary layer reforms). By adding more support (spacer) grids at smaller intervals along the rod bundle one could increase the amount of turbulence present at larger regions in the flow. The downside of this would be the

increased pumping power necessary to maintain the flow rate because of pressure losses. Pressure drop correlations for several common rod bundle support grids were developed in an experimental study by Rehme (1972). Here, the pressure drops for these support grids were measured by using a flow loop and pressure taps connected to U-tube manometers. The flow rate was controlled by using a combination of throttling and bypassing. Data was taken at several different Reynolds numbers for the most common support grid geometries and wire wrap type spacers. From this data, friction factors, loss coefficients and pressure drop correlations were developed and found to be valid for the fuel element spacers in question.

Turbulent flow is a known contributor of enhanced convective heat transfer. Since increased turbulence is present in rod bundle subchannels near the support grids, studying its effects has been worthwhile in understanding theses types of flows. Turbulent mixing was measured using a new experimental method called “thermal tracing” in a work done by Silin, Juanico and Delmastro (2004) , Here thermal traces were produced by using heater-rod units fabricated from nickel alloy strap electrodes. Heat flux values of 5×10^5 W/m^2 and 2×10^5 W/m^2 were used for the highest and lowest flow rates respectively in order to avoid the formation of an air-vapor phase near the heating surface. Dual, high thermal stability current sources along with platinum thermal resistance thermometers and digital amplifiers were chosen for temperature measurements. For case 1, the central subchannel and 3 peripheral subchannels (3 rods) the new technique was found to be highly accurate. The dimensionless Stanton number was found to be independent of Reynolds number, temperature profiles were shown to be fully developed and mixing

rates were all measured to a minimum of 90% accuracy. The findings in the study are similar to past results.

One of the driving mechanisms behind enhanced heat transfer in rod bundle flows is the exchange of mass, momentum and thermal energy between adjacent subchannels (lateral flow fields). This phenomenon is not found in normal circular cross-section pipe flows. The process is referred to as “intersubchannel” mixing or turbulent transport by many researches. The contours for turbulent velocities and kinetic energy were found to have coherent structures which seem to be centered on the region between the corner of the section and the rod. The contours also seem to be parallel and asymmetric. These results were found by Guellouz and Tavoularis (2000), for the case of a single rod in a rectangular channel. Measurements were taken using hot wire anemometry and flow visualization was done by the injection of smoke. This study further and more closely examined the work of Kraus and Meyer (1998). Unlike the research done by Guellouz and Tavoularis, the Kraus and Meyer study involved a large 37 rod triangular array bundle contained within a hexagonal section. Using hot wire probes and thin foil resistive heating elements they were able to effectively measure turbulence intensities and kinetic energy for each central subchannel in the bundle. Results from the experiment showed that turbulence intensity is at its maximum value near the rod surface and gradually decreases when moving toward the center of the subchannel. This is also known to be true when examining azimuthal or axial turbulence intensities. Moller et al. (1991) also noted that turbulence intensity increases as gap size decreases or where there is more near surface flow. Stemming from this effect, Moller et al. (1991) theorized that large eddies were present in the regions of the subchannel near the rod surface. Flow pulsation or

intersubchannel mixing as we have come to know them, are thought to occur because of these eddies in the flow regions near the rod surface. Another theory by Moller (1991) suggested that flow pulsations are one of the driving mechanisms behind flow-induced vibrations of the rod bundle. Interestingly enough its was also found that wall shear stresses and wall temperatures varied over a much greater range when comparing central channel flows of different pitch to diameter (P/D) ratios and even more so when directly comparing to normal pipe flow. The 2 ratios chosen for the study were 1.06 and 1.12. At the largest ratio (1.12) and the maximum distance from either rod surface, turbulence properties were shown to be more similar to normal circular cross section pipe flow. A study by Stovall (2007) investigated the decay of average turbulent kinetic energy density downstream of a split-pair mixing vane support grid. The vane angles were modified using a special made tool for angles of 21° and 37°. It was discovered that a vane angle of 29° promoted more turbulence at larger axial distances downstream. Results were obtained using particle image velocimetry (PIV) and analytical methods. De' Crecy et al. (1994) investigated subchannel mixing coefficients for rod bundle with the standard and mixing vane support grids. It was discovered that the mixing coefficient for a mixing vane grid was ten times larger than that of a standard (vaneless) support grid.

Single Phase Heat Transfer

The performance of a pressurized water reactor is limited by the maximum fuel rod surface temperature and critical heat flux (CHF). Fuel rods tend to corrode at higher temperatures and can be easily damaged in this state. Also, at this temperature the coolant (usually pure water) is unable to prevent phase change. This state is usually referred to as departure from nucleate boiling (DNB). In order to prevent such dangerous scenarios as

rod dryout, accelerated surface corrosion and even melting, efforts have been placed on methods to increase the critical heat flux of the reactor.

By enhancing the single phase heat transfer for a rod bundle flow one can significantly raise the CHF. The most common method is adding features to the support grid that delay the formation of vapor bubbles on the rod surface. Also, since there is more lateral flow the vapor bubbles tend to be swept into the center of the subchannel where they are likely to collapse. Vapor bubbles adhering to the rod surface will effectively insulate that area of the rod and cause it to heat to extreme temperatures. Studies concerning DNB/CHF also found that the flow manipulations greatly increased the single phase heat transfer coefficient as a byproduct. Adding flow enhancing features to a standard support grid, such as disc or mixing vanes created coherent flow conditions that served to increase cooling several hydraulic diameters (D_H) downstream of the support grid. The Holloway et al. study (2005) effectively demonstrated that a support grid with disc would enhance the single phase heat transfer slightly in comparison to other grid designs. However, the flow blockage and pressure losses for this grid are detrimental to the system as a whole. With less blockage than a disc and more heat transfer enhancement than no features at all (standard grid), split-pair mixing vanes are the most ideal candidate for improving heat extraction in rod bundle flows. Mixing vanes are arranged on the support grid so that swirling flow is produced in each subchannel. Split-pair mixing vanes also help to promote intersubchannel mixing and flow impingement on the surface of adjacent rods. This was confirmed is several past studies. Ikeda et al. (2006) used a computational fluid dynamics (CFD) model to directly correlate lateral velocities and enthalpy around the rod surface. It was shown that the split-pair

mixing vanes are the main factor in distributing thermal energy downstream of the support grid. The simulation here modeled a 5 x 5 rod bundle that contained alternating mixing vanes and standard support grids at equal intervals. Another Holloway study (2005) investigated the azimuthal variations in heat transfer for different support grid designs. It was discovered that split-pair mixing vanes enhanced heat transfer more effectively than standard grids but also caused “hot streaks” to develop on the rod surfaces. A vaned support grid had up to a 30% variation in the Nusselt number around the rod’s surface while a high blockage disc grid had a near uniform distribution of only a 4% maximum variation. A standard support grid had up to a 16% variation in heat transfer. Comparison of experimental and CFD data showed that the large spikes in the distribution were caused by flow impingement while the low heat transfer regions (hot streaks) were caused by near stagnant axial flow stemming from flow separation on the rods surface.

CHAPTER THREE
EXPERIMENTAL FACILLITY

The experimental facility used for this project mainly consists of 4 major subsystems. The flow apparatus, assembled fuel rod bundle, electrical components and digital data acquisition software.

Flow Apparatus

The flow assembly serves the purpose of controlling the amount of air being drawn over the heated fuel rod bundle. It also includes air to water heat exchangers which keep the ambient air temperature in the laboratory at a relatively steady value. Ambient air enters and is filtered in the inlet plenum (Figure 3.2). The inlet plenum has 2 thermocouple ports that measure the inlet temperature and a large panel type air filter which blocks airborne particles over 1 micron in size. The now filtered air flows through a 5in diameter PVC pipe to the Laminar flow element (LFE, Meriam 50MC2-4) that is connected to manometers for flow rate measurement purposes. From there, the air passes through a large gate valve which can be manipulated to control the flowrate (Figure 3.1). It must be noted that for all data taken during this project the gate valve was left in the fully open position for maximum flow. The air now makes a right turn by way of a large T-fitting and enters into the test section (Figure 3.1). Here, air flows over the partially heated 5x5 rod bundle. The test section has a length of 1.7m, a square cross section ($42.6cm^2$) and is constructed of lexan. Polystyrene sheets are placed over each side of the test section to minimize heat losses to the outside environment. The assembled rod bundle protrudes through both ends of the test section (Figures 3.2/3.11) for electrical connection purposes. In order to seal the rod ends on the end flanges of the test section, a

combination of 3 acrylic plates are used. The first 2 plates have provisions for o-rings on every other rod. There was insufficient space in between each rod for o-rings to be placed entirely on one end plate. The final plate is fastened down which compresses each o-ring into place. A 4-way fitting is placed at the downstream end of the test section with 1 end sealed off using the aforementioned plates; the air now splits into opposite paths. Two thermocouples are placed at each side of the 4 way fitting to measure exit air temperatures. Now, the air enters into a heat exchanger where it is cooled before entering the compressor. The compressor (17 HP) is a Fuji liquid ring type which has a high enough pressure ratio to provide Reynolds numbers up to 35,000. Next, the air exits the compressor and flows into a diffuser to minimize pressure losses. Finally, an additional heat exchanger is used to cool the air down to near ambient levels. The water flow for both heat exchangers is provided by a small electric centrifugal pump (3hp). A diagram of the flow facility is shown in figure 3.1.

Rod Bundle Assembly

The fuel rods used for this experiment are nearly identical to those used in industrial pressurized water reactors. Each rod has a nominal diameter of 9.5mm and a length of about 2.7m. In order to simulate heat released from a fission reaction, direct resistance heating was utilized. To achieve this, each rod is comprised of 3 sections. The outer rod ends are low resistance (2mΩ) nickel 200, with a length of .85m, while the center section is inconel tubing which has a much larger resistance (130mΩ) with a length of 1m and wall thickness of .38mm. The 3 sections are joined together with high temperature silver solder. The square array rod bundle is assembled using 5 support grids. The 3 center support grids are the split-pair mixing vane test grids in question (Figures

3.5/3.9). Measurements were taken in the distance between the latter 2 downstream support grids where the flow is fully developed. The remaining 2 standard grids are placed near the ends of the test section.

Modification of the vane angles was achieved using a custom designed tool (Figures 3.6/3.8). The vane angle tool is a small device with a slotted end that is placed over the vane. The user places a small amount of force on the end of the tool which in turn creates enough bending moment to alter the vane angle. The angle is then verified using cylindrical gauge blocks which fit squarely in the support grid (Figures 3.7/3.8). A gauge block installed in the support grid is depicted in figure 3.10. The angles were visually inspected at 2x magnification to ensure a high level of accuracy. High precision electro-discharge machining was used to fabricate both the angle gauges and tool. Stainless steel was selected for its dimensional stability and corrosion resistance. The finished products are shown in Figure 3.8. The angles were modified for each vane on each of the 3 support grids (Figure 3.9). The assembled 5x5 rod bundle has the exact pitch to diameter ratio (P/D) of a large industrial 17x17 rod bundle. The P/D for the rod bundle used in this experiment is 1.32. The instrumented rod in the center location allows for temperature measurements. The instrumented rod houses the sensor within its center inconel section. Here the sensor can be displaced or rotated to measure any temperature in any location on the I.D. of the rod. Conductions effects are negligible because of the thin wall tubing. The sensor is constructed of 4, 30 gauge, E-type thermocouples positioned 90° apart (Figure 3.11). Each thermocouple is spot welded to a small steel spring that presses against the inside wall of the tubing. The springs have a width of 1.6mm, so any thermocouple readings will actually represent an average of the

temperatures from a 20° section of the inner rod surface. The sensor positioning rod allows for manual actuation of the sensor position and it also houses the necessary wiring for each thermocouple. Shrink tubing was used to insulate the positioning rod from the inconel/nickel rod section and ensure a snug fit. A slotted bracket is fastened to the end of the positioning rod along with a protractor. The bracket rides on an aluminum channel fixture that has a scale for axial measurements. The aluminum channel and positioning rod bracket are adjustable so that the instrumented rod can be placed in any location within the rod bundle (Figure 3.7). For this particular study, all measurements were taken on the center rod (rod 13).

Current from an Omega (5v, 875amp) power supply was channeled into the rod bundle using six 1/0 welding cables and a power distribution block for each. From the power distribution block smaller gauge wires are connected to copper plates that are placed over the rod bundle ends (Figure 3.12). An HP multimeter was used for current/voltage verification. Temperature data was taken using a 16bit digital data card along with the appropriate data acquisition software (Pdaqview).

Experimental Method

The Pdaqview software was configured to record 25 data points at each angular position/location with a scan rate of .75Hz. These values were then averaged for data reduction purposes. As previously stated, the sensor rod was rotated in 22.5° increments to gather data at 16 angular positions at each axial location. All temperature measurements were taken in the range of axial locations from $-5D_H$ and $40D_H$ with respect to the downstream edge of test support grid #2. For 20 different axial locations, this yields a total of 80 individual data sets, with each data set containing multiple

inlet/outlet and rod surface temperatures. Voltage and current were manually recorded at each data set location using the multimeter and power supply respectively. To ensure repeatable results, voltage and current were set to approximately 4v and 700amps respectively. The maximum available flow rate was utilized for each data test. The flow apparatus and direct resistance heating components were allowed to reach steady state before recording data. The steady state condition was verified by visually inspecting a live view of the temperatures within the rod bundle.

Uncertainty Analysis

The thermocouples used for obtaining temperature measurements in this experiment were calibrated in the range of 20° to 70°C (13 pts) using an RTD (Omega PRP-1) and a benchtop thermometer (Omega DP251) as the standard. Each thermocouple was corrected based on a least squares fit of the calibration data at their respective DAQ channels. The resultant uncertainty for thermocouple measurements were evaluated using the respective errors for the calibration equation, RTD, reference junction compensation and A/D converter. This value of ±.11°C was determined from equation 3.1. Random uncertainty in temperature measurements was eliminated during data reduction by time averaging the instantaneous temperatures. The standard deviation for instantaneous temperature measurements was negligible.

$$un_T = \sqrt{\left(un_{T,cal}^2 + un_{T,RTD}^2 + un_{T,ref}^2 + un_{T,A/D}^2\right)} \tag{3.1}$$

A total uncertainty of ±3.5 CFM was determined for the actual volumetric flowrate (Q_{ACFM}). This value is obtained based on the calibration error ($Q_{ACFM,cal}$) and the resolution error ($Q_{ACFM,acc}$).

$$un_{Q_{ACFM}} = \sqrt{un_{Q_{ACFM,cal}}^2 + un_{Q_{ACFM,acc}}^2} \tag{3.2}$$

The uncertainty of the mass flow rate was found to be ±0.002kg/s.

$$un_{\dot{m}} = \sqrt{\left(\frac{\partial \dot{m}}{\partial Q_{ACFM}} un_{Q_{ACFM}}\right)^2 + \left(\frac{\partial \dot{m}}{\partial T_f} un_{T_f}\right)^2 + \left(\frac{\partial \dot{m}}{\partial P_f} un_{P_f}\right)^2} \tag{3.3}$$

Heat flux was calculated directly from the inlet/outlet temperatures and mass flowrate rather based on the current/voltage measurements. This method was chosen to avoid any errors associated with any heat losses outside of the test section. The uncertainties of the rod bundle surface area and specific heat of air were evaluated and deemed insignificant. The total uncertainty for the calculated heat flux was obtained using the following relation.

$$un_{q''} = \sqrt{\left(\frac{\partial q''}{\partial \dot{m}} un_{\dot{m}}\right)^2 + \left(\frac{\partial q''}{\Delta T} un_{\Delta T}\right)^2} \tag{3.4}$$

The uncertainty for the calculated heat flux was found to be 8%.

Spatial uncertainties for angular and axial positioning were minimal. Temperature gradients on the rod's surface were much lower than spatial uncertainties. All results were completely repeatable. Slight deviations in positioning had no discernable affect on the obtained results.

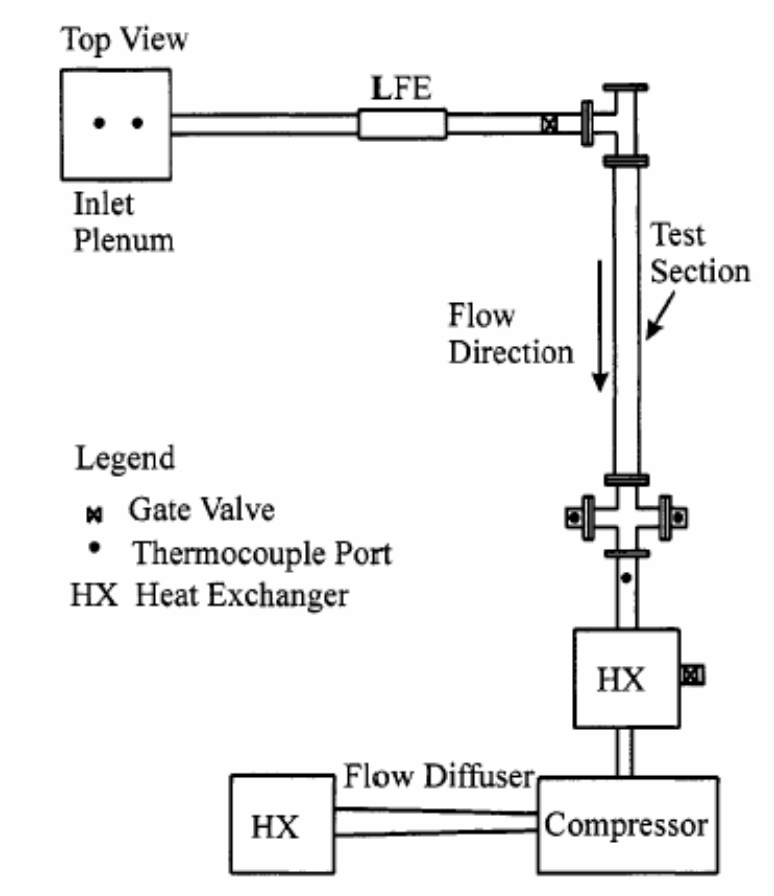

Figure 3.1: Flow apparatus schematic

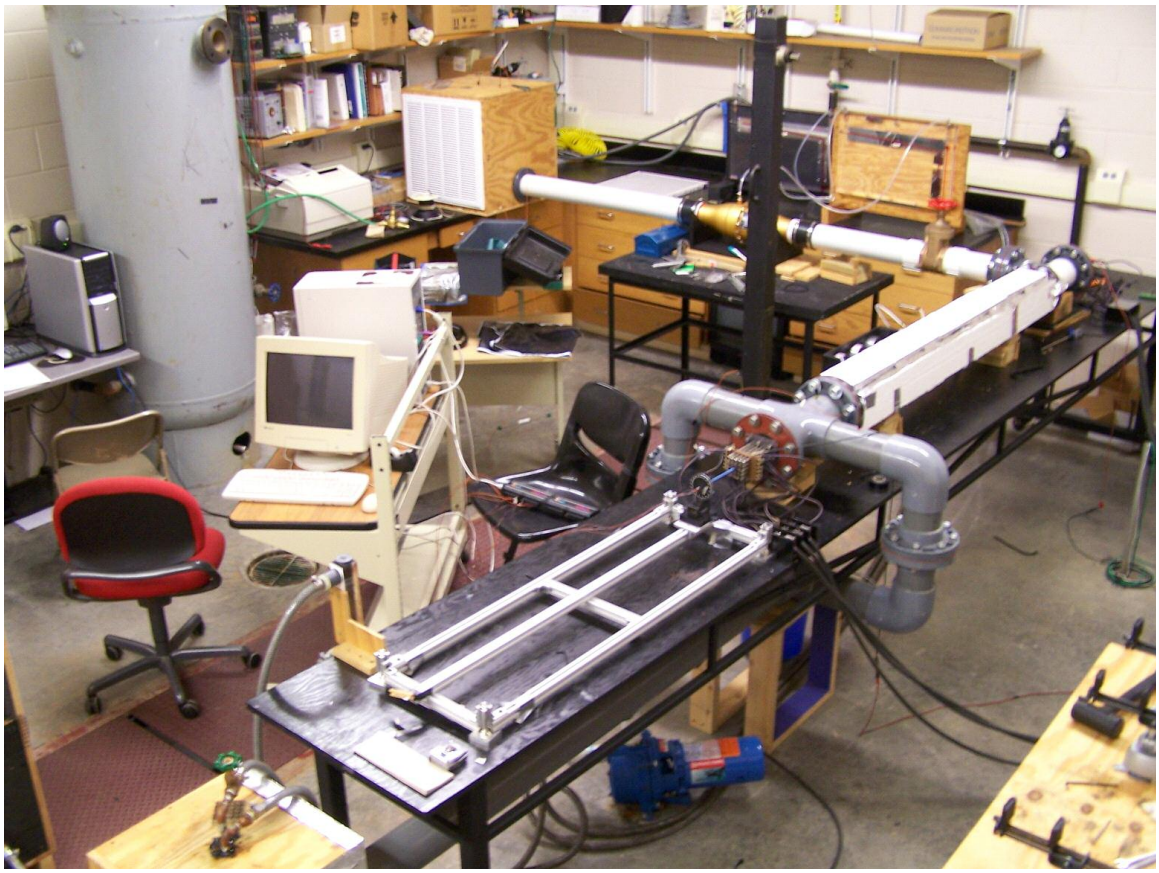

Figure 3.2: Photograph of the Flow Facility

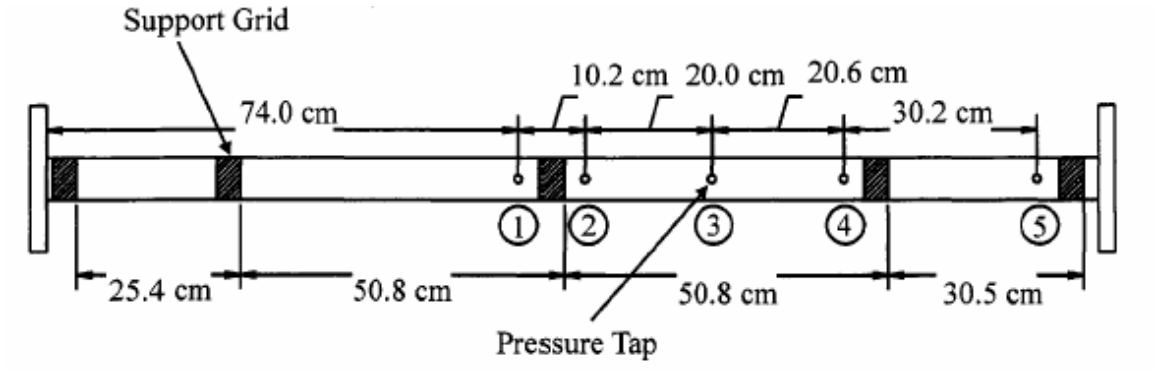

Figure 3.3: Rod bundle Support Grid Locations

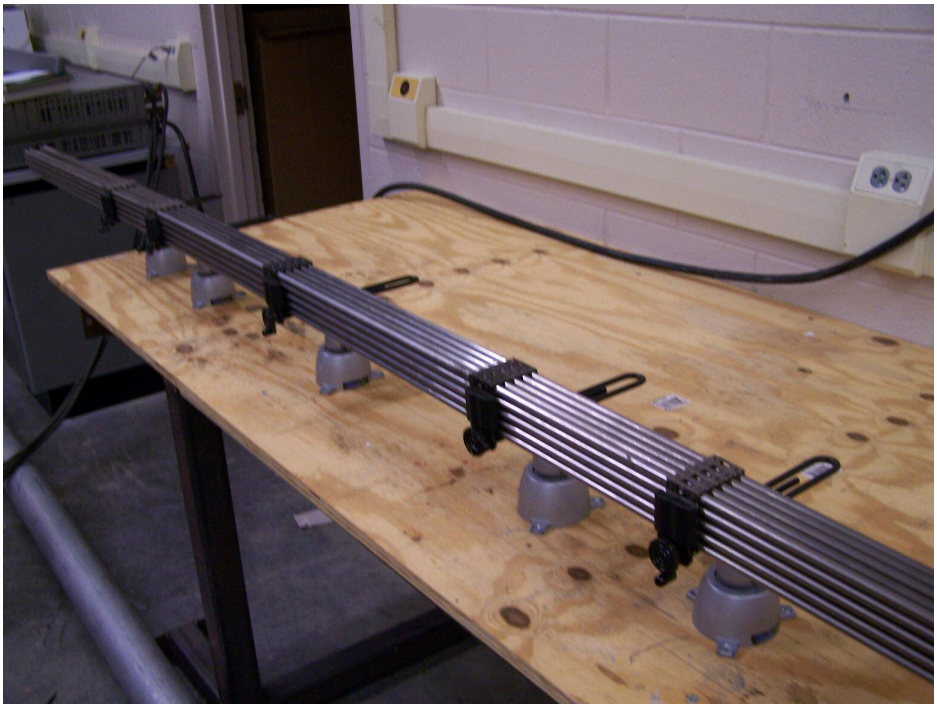

Figure 3.4: Photograph of the Assembled Rod Bundle

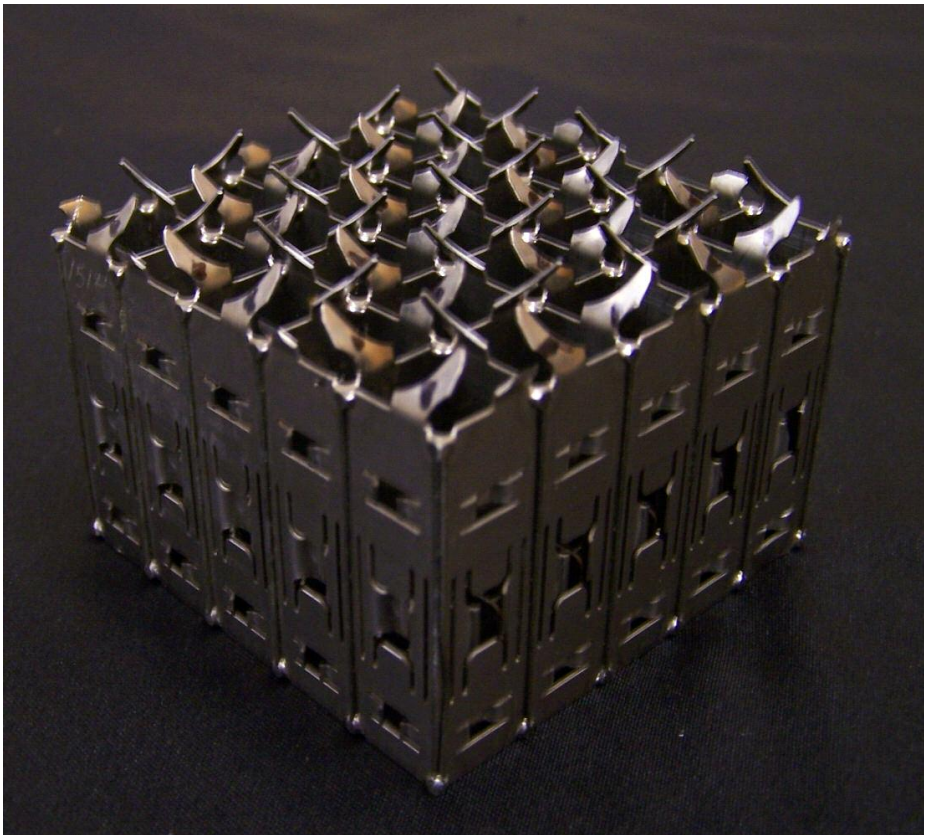

Figure 3.5: Photograph of the Test Support Grid w/ Split-Pair Mixing Vanes

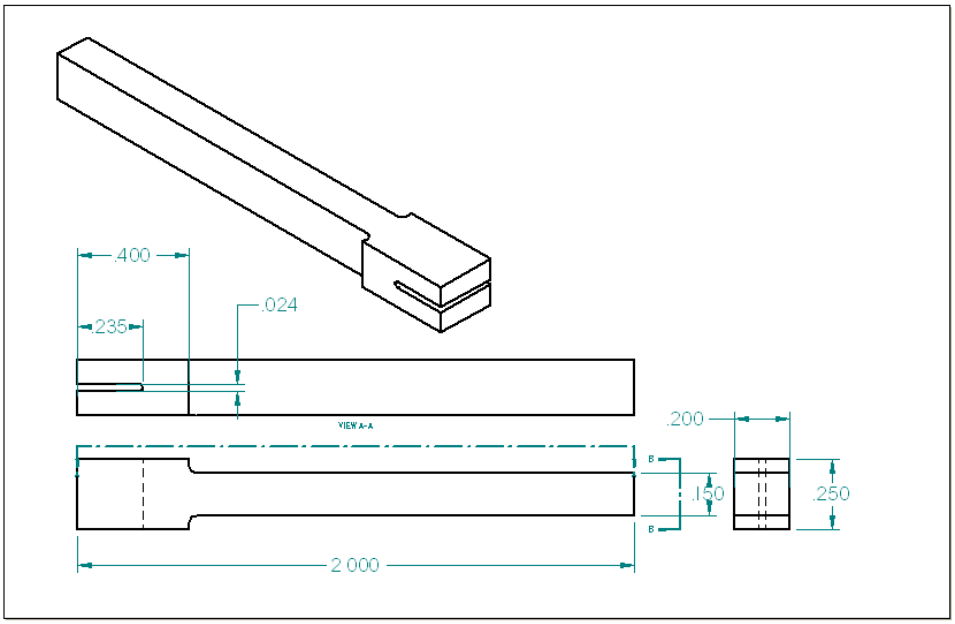

Figure 3.6: Vane Angle Tool

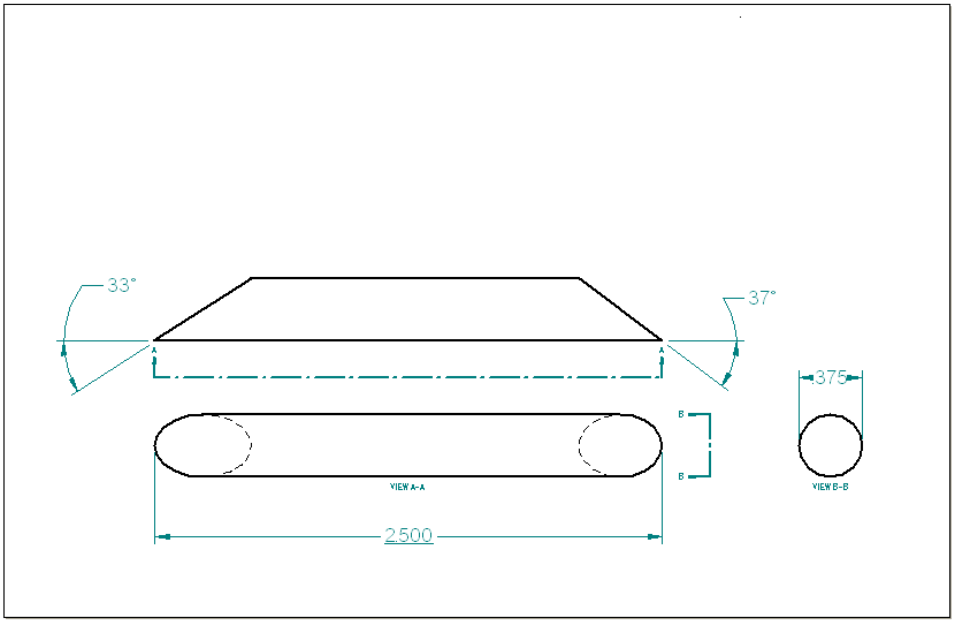

Figure 3.7: Dual Angle Gauge (37°, 33°)

Figure 3.8: Photograph of the Vane Angle Tool/Gauge set

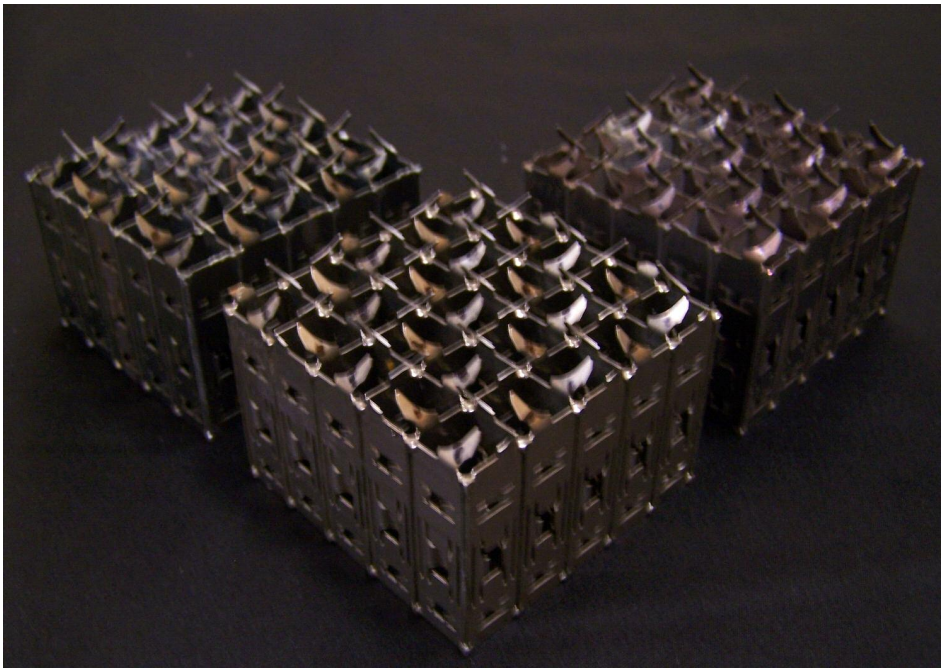

Figure 3.9: Photograph of the Test Support Grids

Figure 3.10: Photograph of Support Grid w/ Gauge Installed

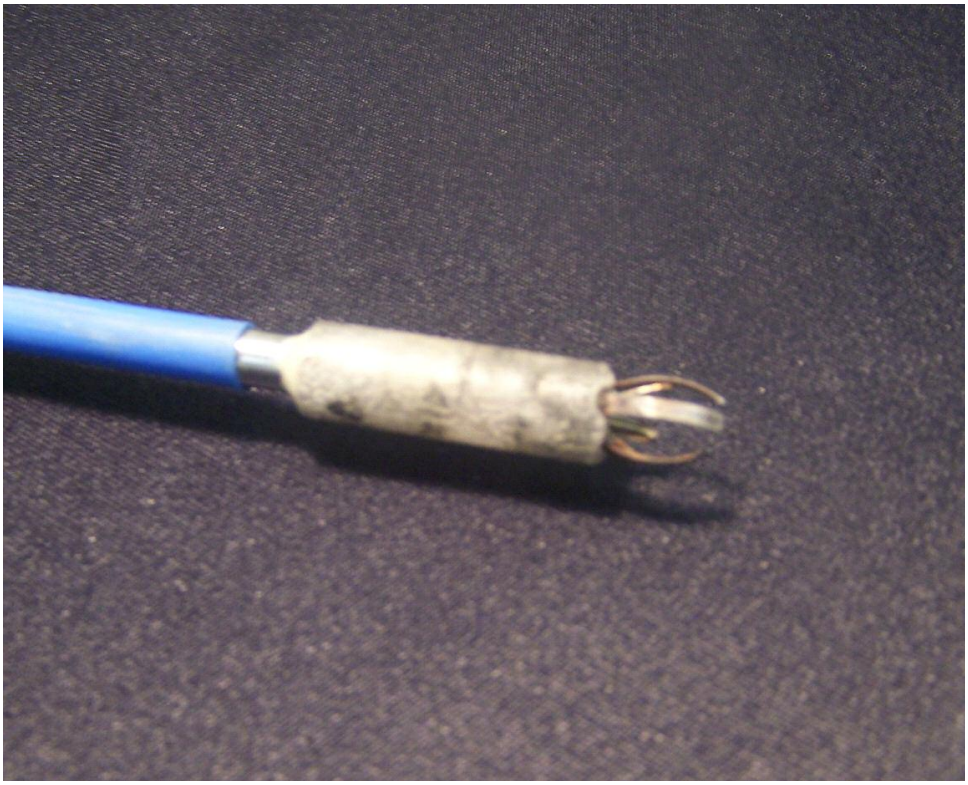

Figure 3.11: Photograph of the Sensor Rod

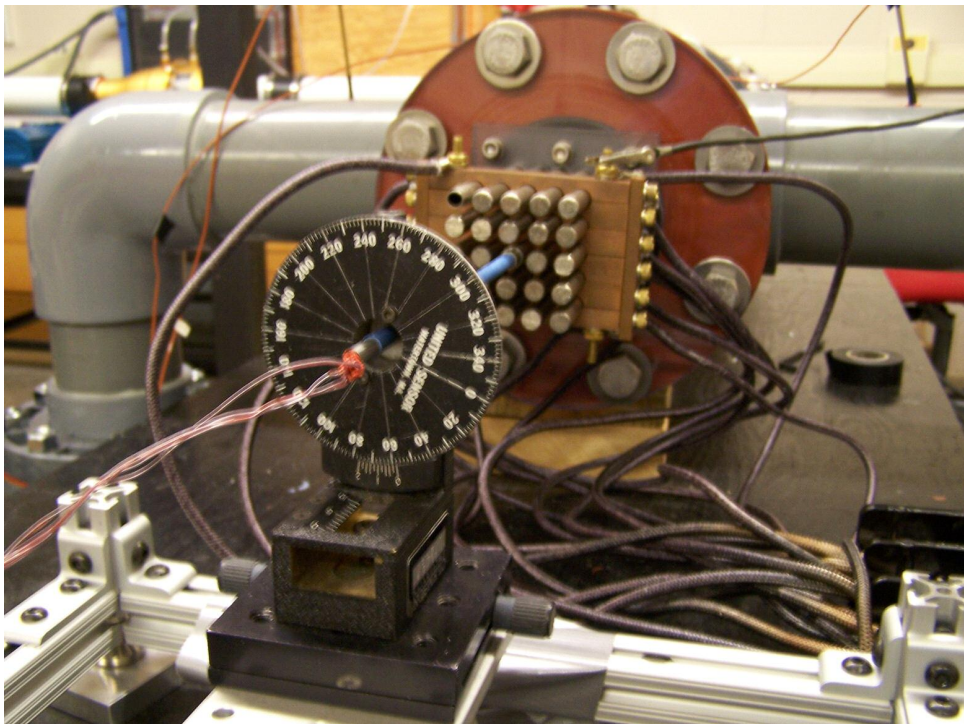

Figure 3.12: Photograph of Rod Bundle w/ Copper Connection Plate

CHAPTER FOUR
DATA ANALYSIS

The pre-calibrated laminar flow element allows for simple determination of the flow rate. By using the laminar flow elements calibration curve and the pressure drop from the manometers we can obtain the actual volumetric flow rate (Q_{acfm}). Since the calibration curve only applies to dry air at standard temperature and pressure, a correction is necessary that corresponds to the existing atmospheric conditions. Using the atmospheric pressure (P_f), the humidity ratio (ρ_{wet}/ρ_{dry}) and the ambient air temperature (T_f), the standard volumetric flowrate (Q_{scfm}) was obtained using the following relation. Ambient temperatures in the laboratory ranged from 22 °C to 26 °C during all testing.

$$Q_{scfm} = Q_{acfm}\left(\frac{\rho_{wet}}{\rho_{dry}}\right)\left(\frac{P_f}{P_{stnd}}\right)\left(\frac{T_{std}}{T_f}\right) \tag{4.1}$$

Using the standard volumetric flow rate one does not have to evaluate the mass flow rate based on the temperature dependent density of wet air. The standard mass flow rate was obtained by simply using the standard density of air shown below.

$$\dot{M}_{scfm} = Q_{scfm}\left(\rho_{stnd}\right) \tag{4.2}$$

The characteristic dimension for a rod bundle subchannel flow is the hydraulic diameter (D_H). The hydraulic diameter is based on flow area and the wetted perimeter (P) of a subchannel.

$$D_H = \frac{4A_{sc}}{P_{sc}} \tag{4.3}$$

The blockage ratio (ε_g) is defined as the ratio of the projected frontal area of the support grid and the open flow area of the subchannel (A_{rb}).

$$\varepsilon_g = \frac{A_{sp}}{A_{rb}} \tag{4.4}$$

The Reynolds number for a rod bundle flow is based on the dynamic viscosity (μ) of air evaluated at its film temperature along with the mass flow rate, hydraulic diameter D_H and open flow area of the rod bundle ($A_{\mathbf{rb}}$).

$$\mathrm{Re} = \frac{(M_{scfm})D_h}{(\mu)A_{rb}} \tag{4.5}$$

Heat flux was evaluated by applying the 1st law to the heated section of the rod bundle. Using the inlet and outlet temperatures the following relation was derived.

$$q'' = \frac{\dot{M}_{SCFM}\, C_P (T_{out} - T_{in})}{RB_A} \tag{4.6}$$

Where Cp is the specific heat of air at standard conditions and RB_A is the total heated surface area of the rod bundle. The bulk air temperature (T_B) is obtained using the same relationship but is derived as a function of axial location (X). P_{RB} denotes the wetted perimeter of the rod bundle.

$$T_B = \frac{q''(P_{RB})(X)}{M_{SCFM}(C_P)} + T_{in} \tag{4.7}$$

The single phase heat transfer coefficient (HTC) and its corresponding Nusselt number (Nu), are evaluated at the film Temperature (T_f) which is simply the average of the bulk air and rod surface temperatures (T_s). The rod surface temperature was directly calculated from raw experimental data by averaging all the temperatures at different angular locations for a given axial position.

$$T_f = \frac{T_B + T_S}{2} \tag{4.8}$$

Using the following relation the single phase heat transfer coefficient (circumferential average) was estimated.

$$HTC = \frac{q''}{(T_S - T_B)} \tag{4.9}$$

Lastly, the circumferentially averaged Nusselt number was obtained using the single phase HTC and the thermal conductivity of air (K) at T_f.

$$Nu = \frac{(HTC)(D_H)}{K} \tag{4.10}$$

CHAPTER FIVE
RESULTS & DISCUSSION

The present study includes results from a parallel work by Stovall (2007) and past research done by Holloway (2005). These works include data that is highly valuable to this project. For this reason, the findings from these studies are presented here to more thoroughly justify the obtained results.

Lateral flow fields

Particle image velocimetry (PIV) was done to obtain the lateral velocity flow fields for several different axial locations in the rod bundle. The PIV results pertinent to the present study are those implementing support grids with split-pair mixing vanes and weld nuggets. Data was obtained in the range of Reynolds numbers from 29,000 to 35,000. The split-pair mixing vanes for the support grids used in this experiment are arranged so that swirling flow will be induced in each subchannel (Figure 5.1, Holloway et al. 2005).

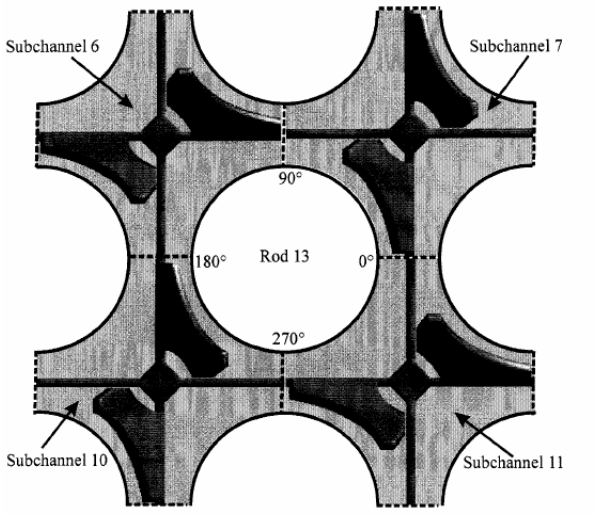

Figure 5.1: center rod subchannel locations

These vanes also direct impinging lateral flow towards adjacent rods. The flow field in the subchannel directly downstream of the support grid (1.5 D_H) contains two counter-rotating vortices. High velocity flow enters the subchannel from the west and exits to the south while weaker flows enter/exit from the north/east. For an axial distance of 5 hydraulic diameters the counter rotating vortices merge to form a large single vortex near the centroid of the subchannel and the varying magnitudes of rod gap exchange flows have near equalized. In the region between 1 and 5 hydraulic diameters very little decay of the lateral flow has taken place. The maximum lateral velocity here is only 3% less than at the axial location at 1 D_H. Further downstream at 10 D_H the large center vortex is still clearly defined although less intense (Figure 5.2, Holloway et al.).

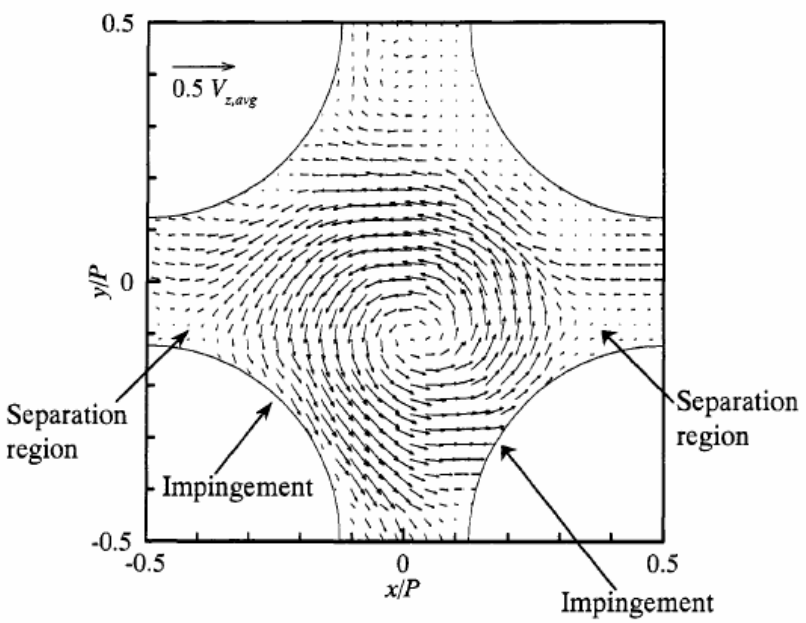

Figure 5.2: lateral velocity field at 10 D∞

The magnitude of the lateral velocities shows that swirling flow is generated strictly because of the geometry of the mixing vanes rather than flow exchange between neighboring subchannels. At this axial location, the largest lateral velocity is only 29% of

the bulk velocity. Directly downstream at only 1.5 hydraulic diameters the lateral velocities can be as high as 52%. Also, past studies have shown that no discernable swirling flow is present in subchannels for rod bundles with a standard (vaneless) support grids even though there is a significant amount of intersubchannel mass exchange. The counter-clockwise rotation sense of the vortex also directly relates the down-up pattern of the mixing vanes shown in figure 5.3 (Holloway et al. 2005)

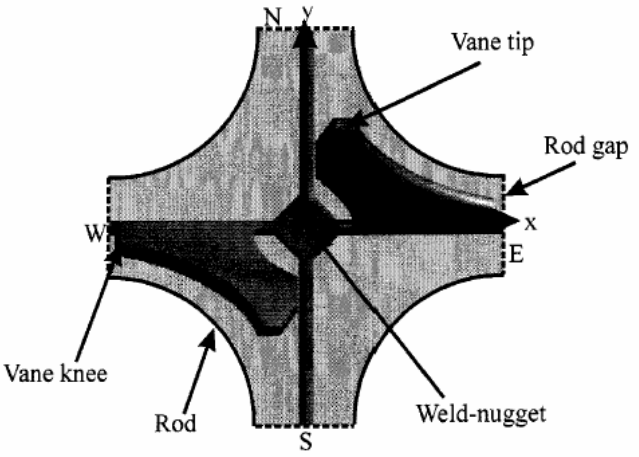

Figure 5.3: split-pair mixing vane pattern

The velocity field in subchannel 6 at 10 hydraulic diameters is shown in figure 5.2 (Holloway et al.). The rotation of the central vortex directs impinging flow towards the southeast and southwest rods. From a subchannel centroid perspective the impingement is most prevalent at the 4 o'clock position for rod 13 and around 8 o'clock for rod 12. These locations represent 45° on the surface of rod 12 and 315° for rod 13 (Figure 5.2, Holloway et al. 2005). It should be noted that lateral flow separation is present on both rod surfaces directly adjacent to the impingement regions. These flow fields were documented for each subchannel surrounding rod 13 (center rod). From a global perspective, the vane pattern encourages flow across subchannels in the entire rod bundle while simultaneously effecting lateral flow conditions downstream. These flow fields are

complex but yet exhibit steadiness. Further downstream of the support grid the large vortices present in the subchannels finally succumb to viscous dissipation and most if not all lateral flow has ceased. Computation fluid dynamic (CFD) simulations are in agreement with experimental data for lateral flow fields in the rod bundle. However, a large amount of error is present in the CFD results because of the lack of wall effects and the use of an infinite array rod bundle.

Using the lateral velocity results obtained from PIV, the average kinetic energy density was calculated.

$$\overline{KE} = \rho_{water} \frac{1}{N} \sum_{j=1}^{N} \left(u_j^2 + v_j^2 \right) \tag{5.1}$$

The average kinetic energy density closely follows the lateral velocities for increased axial distances. Initially, at regions close to the downstream edge of the support grid the average kinetic energy slowly decays as the lateral flow regions are developing. At further axial distances still, where the swirling flow structures are well defined, the decay rate enlarges by roughly 20% (Figure 5.4 Stovall, 2007).

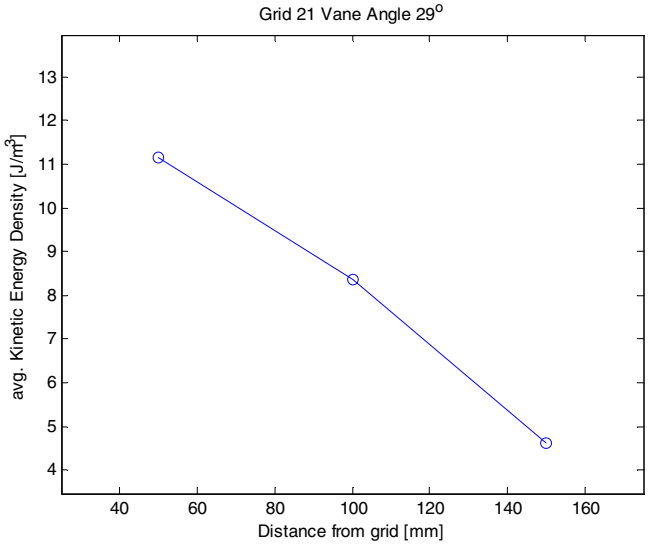

Figure 5.4: Average Kinetic Energy Density @ 29°

For vane angles of 37° and 21° the average kinetic energy density is more preserved and has a lower decay rate but is much lower overall than at 29°. At 50mm from the downstream edge of the support grid strap, the average kinetic energy density is at its maximum level of 11.25 J/M^3 for a vane angle of 29°. The maximum is 7.5 J/M^3 and 5.85 J/M^3 for vane angles of 33°, 21° degrees respectively. This solidifies the assertion that 29° is the optimum vane angle for subchannel flows (Figure 5.5 Stovall 2007).

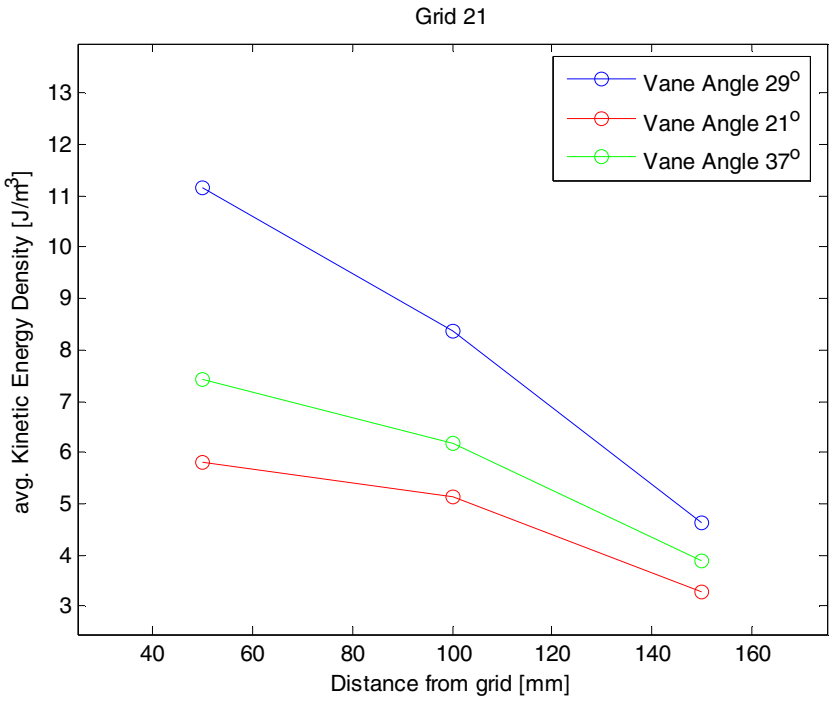

Figure 5.5: Average Kinetic Energy Density @ 21°, 29°, 37°

The difference in average kinetic energy density between the 3 vane angles can be attributed to the amount of swirl and blockage generated in the support grid. The average kinetic energy density for each vane angle is shown on figure 5.5 (Stovall, 2007). Since 21° is more shallow than 29°, the vanes induce less lateral flow in the subchannel and consequently less mixing. A vane angle of 21° also has less flow blockage which is more desirable for axial flow. Flow blockage heavily increases turbulence but causes increased

flow losses. The 33° vane angle has reached the point of diminishing returns as far as swirl is concerned, so again, there is less coherent lateral flow structure development when comparing to 29°. Comparison of data at vane angles of 33° and 21°, the amount of blockage is the governing factor in the average KED. Both vane angles produce less swirl than the optimum angle of 29° but 33° exhibits a slight advantage over 21° because of increased flow blockage. Even with an axial distance of 150mm where the swirling flow structure has greatly diminished, a vane angle of 29° still has more overall average KED. At this distance 29° has roughly 20% more average KED than 33° and nearly 50% more than 21°. The data from CFD, PIV and past studies are in complete agreement. A subchannel flow downstream of a split-pair mixing vane support grid has a coherent swirling structure that extends axially to distances greater than 10 D_H. The angle (29°) and direction of the split-vane mixing pairs are optimized so that there is increased turbulence intensity, mass flow exchange between subchannels and minimized blockage. These aspects of the flow are greatly enhanced over a standard support grid and will allow for increased thermal energy extraction for the entire fuel rod bundle assembly.

Thermal Effects

The rod surface temperatures at 16 different angular locations were averaged in order to obtain the circumferentially averaged heat transfer coefficient. For the baseline test, at a vane angle of 29° the average rod surface temperature increases linearly as expected and becomes parallel with the bulk surface temperature at 25 hydraulic diameters, where the thermal system has reached fully developed conditions (Figure 5.6).

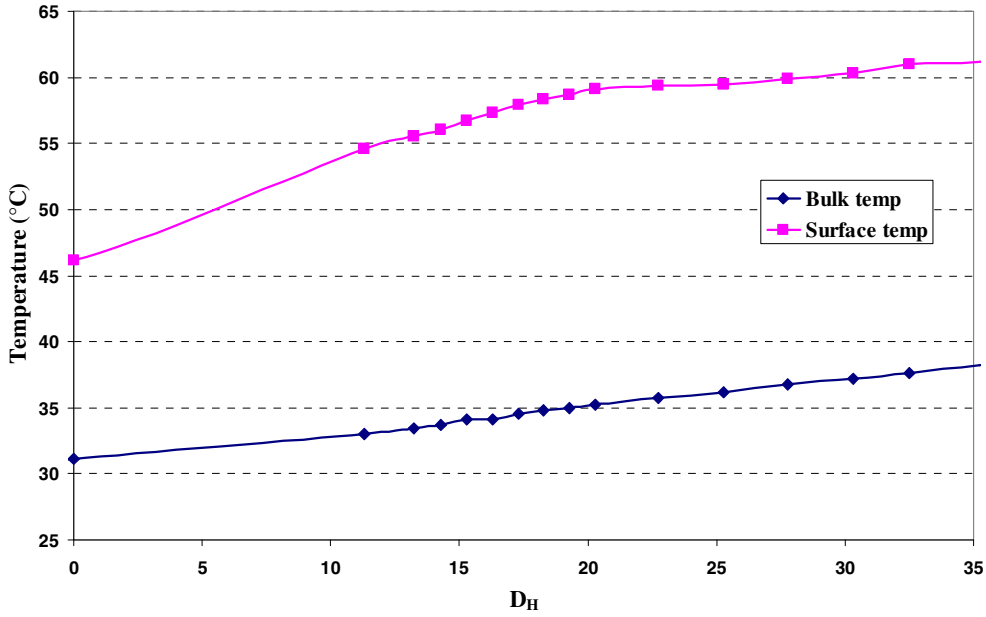

Figure 5.6: Bulk/Surface Temperature development (vane angle 29°)

When examining the heat transfer enhancement for axial locations downstream of support grid 2, it can be seen that the flow conditions are initially highly favorable for heat exchange. At 0 D_H the heat transfer is increased well over 50% of its fully developed value. Moving further downstream it rapidly decreases in a near exponential manner to a distance of 10 D_H where the decay rate abruptly changes. At this location, there is only an enhancement of approximately 9%. Beyond 10 D_H the decay rate has de-accelerated greatly. From 10 D_H to 20 D_H there is only a 10% change in heat transfer enhancement. At axial distances greater than 25 D_H there is virtually no vane geometry dependent lateral flow and consequently 0% enhancement in heat transfer. As the flow approaches the 3rd support grid, the boundary layer is disrupted and there is a slight increase in heat transfer. This effect occurs in the fully developed region and extends to the next support grid at roughly 43 D_H. The normalized Nusselt number for the center rod (13) can be seen in figure 5.7.

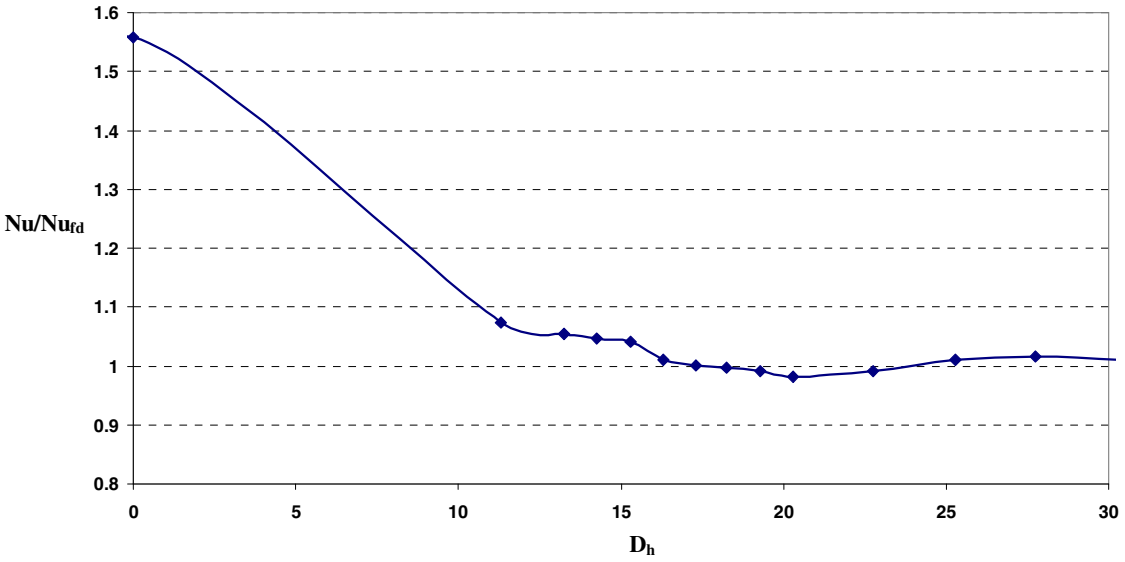

Figure 5.7 Heat transfer enhancement for a vane angle of 29°

Modification of the vane angle causes a tremendous effect on the amount of heat transfer enhancement in the flow. The angles 37° and 33° have maximum heat transfer enhancements that are 20% and 27% lower than 29° (Figure 5.8).

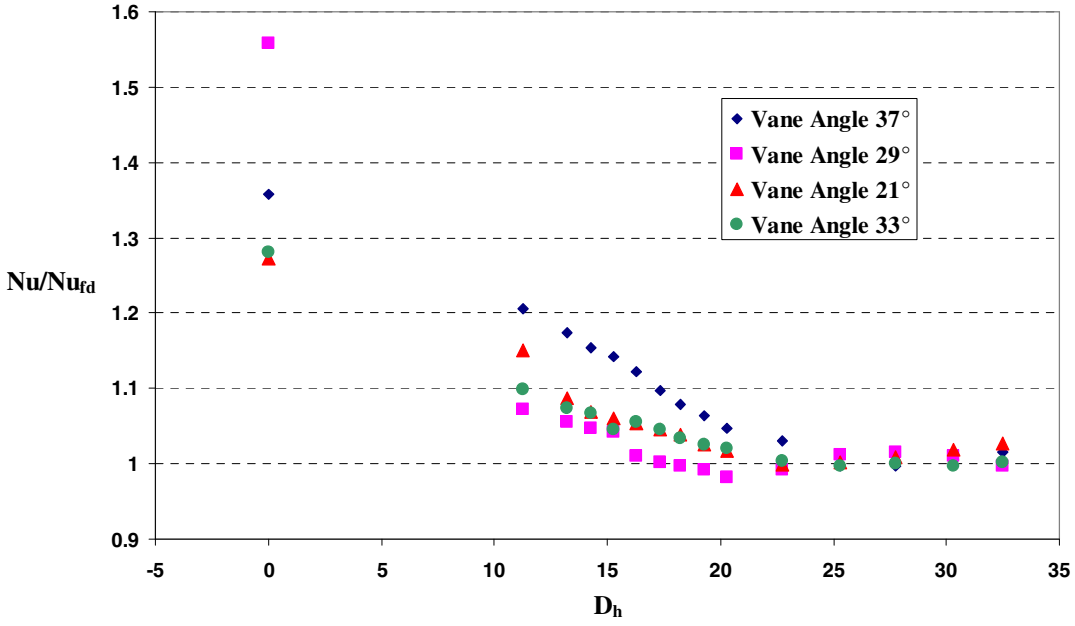

Figure 5.8: Heat transfer enhancement for Vane Angles 37°, 33°, 29°, and 21°

The increased blockage at these angles (37°, 33°) has interfered with the development of swirling flow and intersubchannel mixing. A shallower angle of 21° displays even less prowess in heat transfer enhancement. At 0 D_H there is only a 27% increase in heat transfer. Surprisingly, 21° and 33° degrees have very similar if not identical effects to the to heat transfer enhancement. This stems from the interaction between swirl and blockage. A vane angle of 33° obviously creates more chaotic turbulence than 21° but has less swirling flow. The 2 effects counter-act one another in a way that produces the same overall effect on the heat transfer enhancement in the subchannel. That being said 21° would be more desirable for the fact that it has less flow blockage which would allow for minimal pressure losses. Heat transfer enhancements for each support grid were also predicted using correlations from Holloway et al. (2005) and Yao (1982). These empirical correlations attempt to predict heat transfer enhancements downstream of the support grid based on the grid blockages ratios (ε_g). The blockage ratios for the test support grids at each vane angle are listed in the table below.

Vane Angle	ε_g
37°	.53
33°	.50
29°	.48
21°	.42

Table 5.1: Support Grid Blockage Ratios

These correlations were unable to predict heat transfer enhancement for modified support grids with any acceptable amount of accuracy. Both correlations predicted heat transfer enhancements substantially higher than the measured results. A large amount of error is present in the predictions because the correlation's constants were based on experimental data implementing support grids with a vane angle of 29°.

Temperature data was used to obtain the azimuthal heat transfer variation around the surface of the rod. As stated in chapter 3, a standard support grid has a maximum variation in the heat transfer coefficient of 16%. Since a standard support grid has no flow defining features and is completely symmetrical, the mechanisms driving the temperature variation are not geometry dependent in this particular case. Three main factors cause azimuthal variations for a subchannel flow; pulsating intersubchannel mass exchange, local flow acceleration due to the presence of the grid and also increased turbulence. At 29°, the split-vane mixing pairs direct impinging flow toward the surface of the rods to the south of the subchannel. Next to the regions of impinging flow are regions of axial flow separation. The angular locations of these very contradictory flow conditions directly relate to spikes in the azimuthal heat transfer variation. The 30% increase in the Nusselt number corresponds to the impingement region while a 10% decrease in heat transfer is observed for the stagnant flow region (Figure 5.9, Holloway et al. 2005)

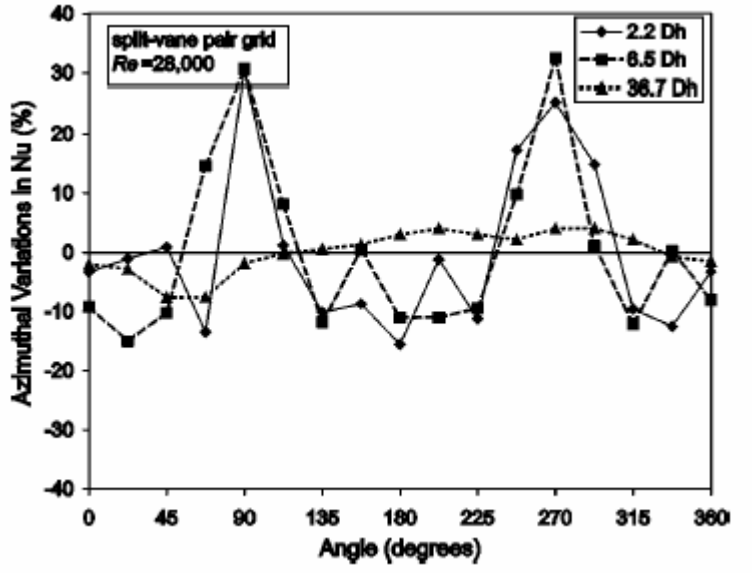

Figure 5.9: Azimuthal Variations in Heat Transfer for a Vane Angle of 29°

Temperature measurements along the I.D. of the center rod surface reveal that flow structure directly related to support grid geometry and/or features has a significant effect on the amount of circumferential heat transfer variations.

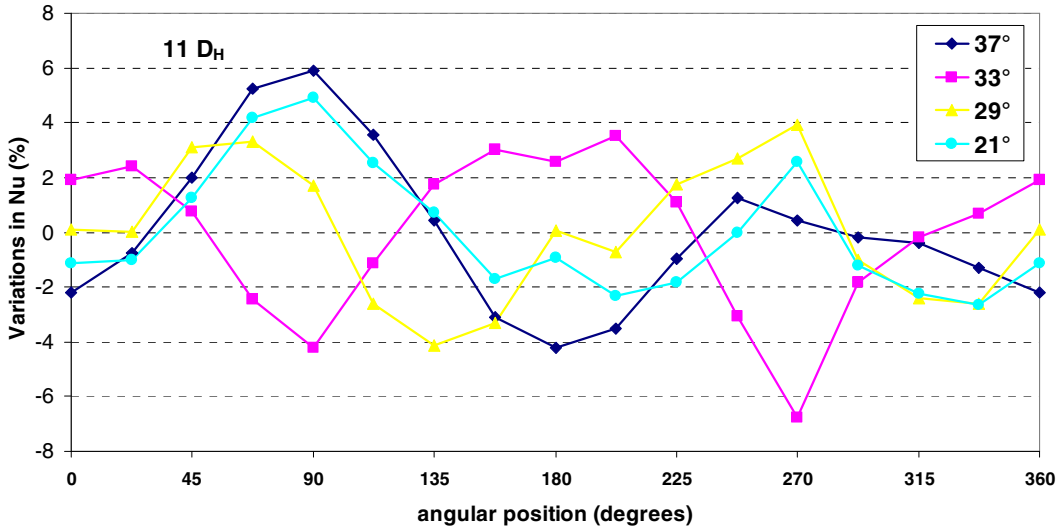

Figure 5.11: Azimuthal Variations in Heat Transfer at 11 D_H

A maximum variation of roughly 10-12% seems to be present at each vane angle. These "spikes" also seem to occur in nearly the same location. Data at vane angles of 37° and 21° seem to track one another closely with nearly the same percent variation at every angle save for 180°. Azimuthal variations in heat transfer at vane angles of 29° and 33° exhibit similar behavior but appear to be slightly out of phase. Examination of azimuthal heat transfer variations at 3 axial locations shows that the behavior, however complex it may be is not random. As expected, the profiles converge further downstream between 11 and 13 hydraulic diameters (see appendix).

CHAPTER SIX
CONCLUSION

Temperature data has been taken on multiple points on the center rod of the bundle. Modifications were made to the vane angles for 37°, 33° and 21°. From this data, the thermal performance of each vane angle was evaluated and compared to results obtained from PIV.

The circumferentially averaged Nusselt numbers for each grid vane angle confirm the assertion that a vane angle of 29° is optimal for promoting swirling flow. Also, the effects of this flow field are greater heat transfer enhancements at increased axial distances from the support grid. Modification of the vane angle has a significant effect on the heat transfer enhancements immediately downstream of the support grid in the region between 0 D_H and roughly 20 D_H. The increased heat transfer in this region is promoted by the presence of the support grid, which causes disruption in the boundary layer growth and localized flow acceleration. Beyond the standard amount of enhancement, heat transfer is further magnified because of the strong lateral flow fields and swirling flow structure from the split-pair mixing vanes. Vane angles more shallow than 29° have less blockage but do not promote swirling flow well. The opposite is true with the less shallow grids. The increased blockage is beneficial for highly chaotic turbulence/mixing but less so for maintaining a coherent swirling flow structure around each rod. The tradeoff between the two causes the same overall affect on the heat transfer enhancements. However, as previously stated a lower blockage grid is more desirable from a global perspective because there is a smaller pressure drop across each grid. At a vane angle of 29° there is a mysterious “dip” in the heat transfer enhancement at an axial

distance of approximately 20 D_H. This phenomenon is not present at the other vane angles. At this time, the underlying mechanism driving this behavior is not known.

Examination of the azimuthal variations in heat transfer at each vane angle shows that there is some interaction between flow structure and “spikes/dips” in local heat transfer around the rod. These slight variations in azimuthal heat transfer can be attributed to geometry dependent flow effects such as flow impingement and regions of flow separation on the rods surface. The results obtained in this study are in complete agreement with past works (Holloway et al. 2005/Stovall 2007).

APPENDIX

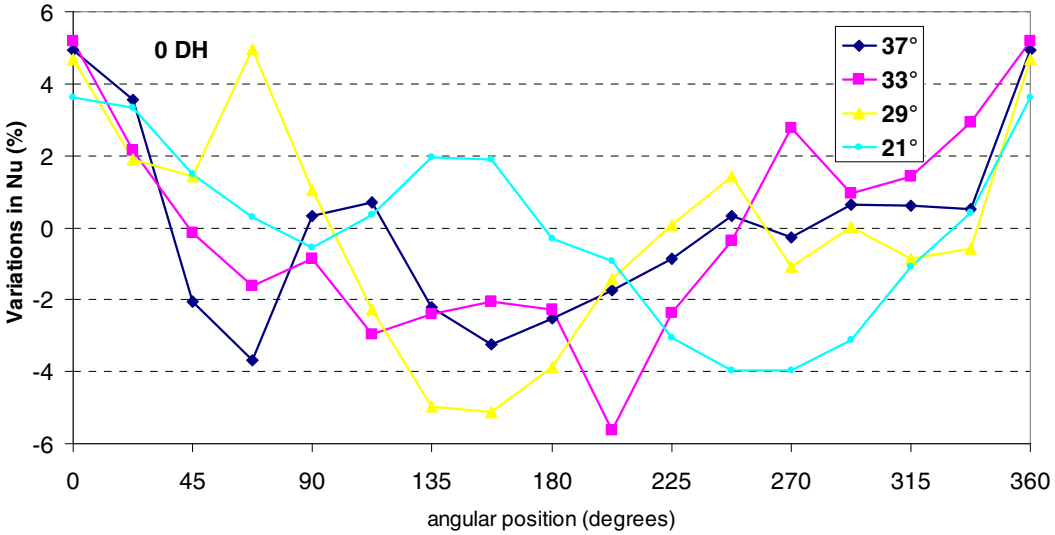

Figure A.1 Azimuthal Variations in Heat Transfer at 0 D_H

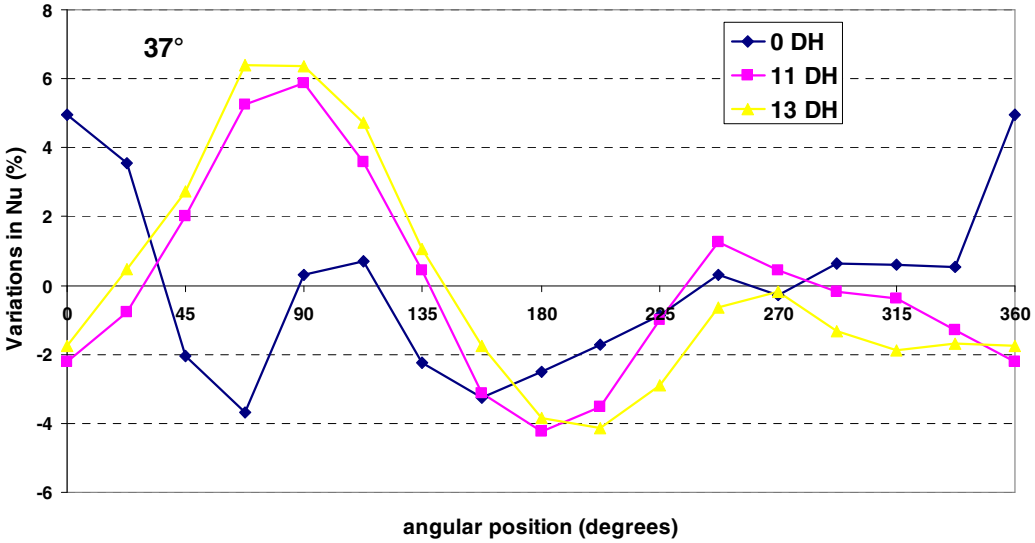

Figure A.2 Azimuthal Variations in Heat Transfer at a Vane Angle of 37°

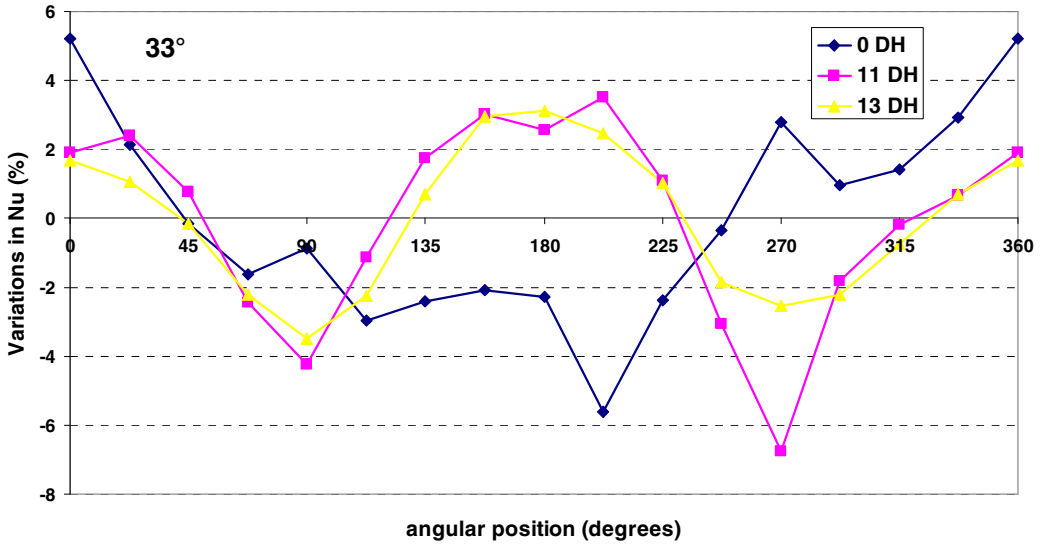

Figure A.3 Azimuthal Variations in Heat Transfer at a Vane Angle of 33°

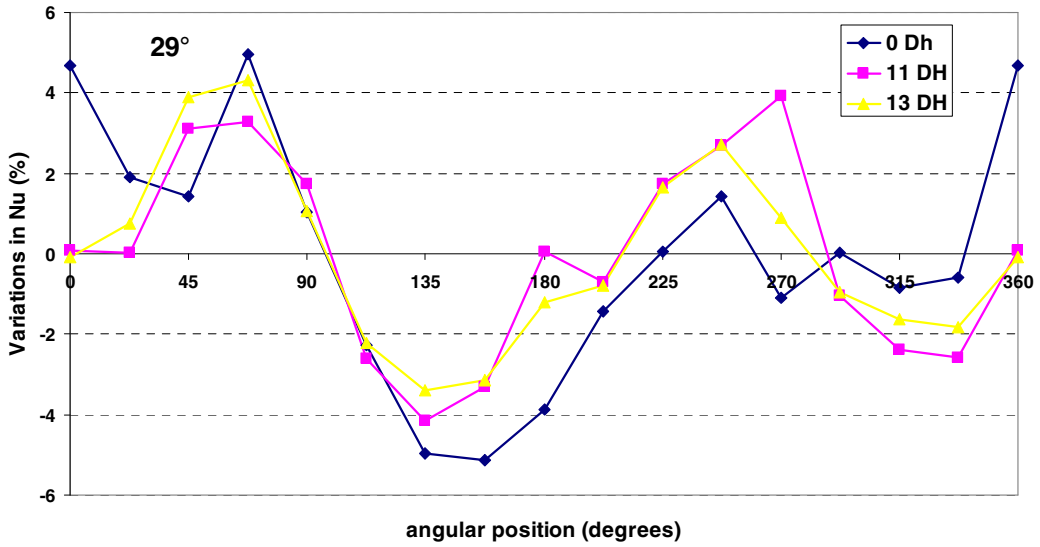

Figure A.4 Azimuthal Variations in Heat Transfer at a Vane Angle of 29°

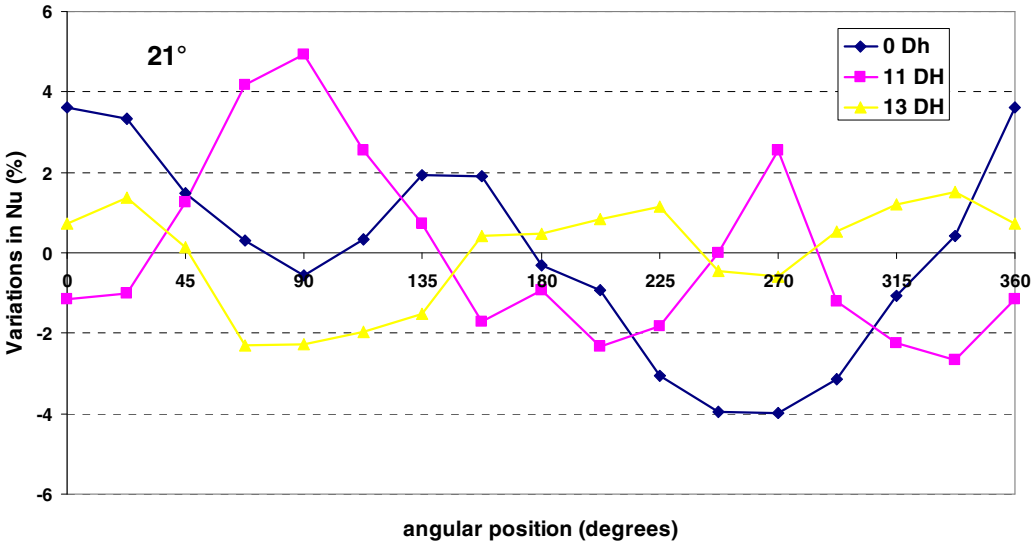

Figure A.5 Azimuthal Variations in Heat Transfer at a Vane Angle of 21°

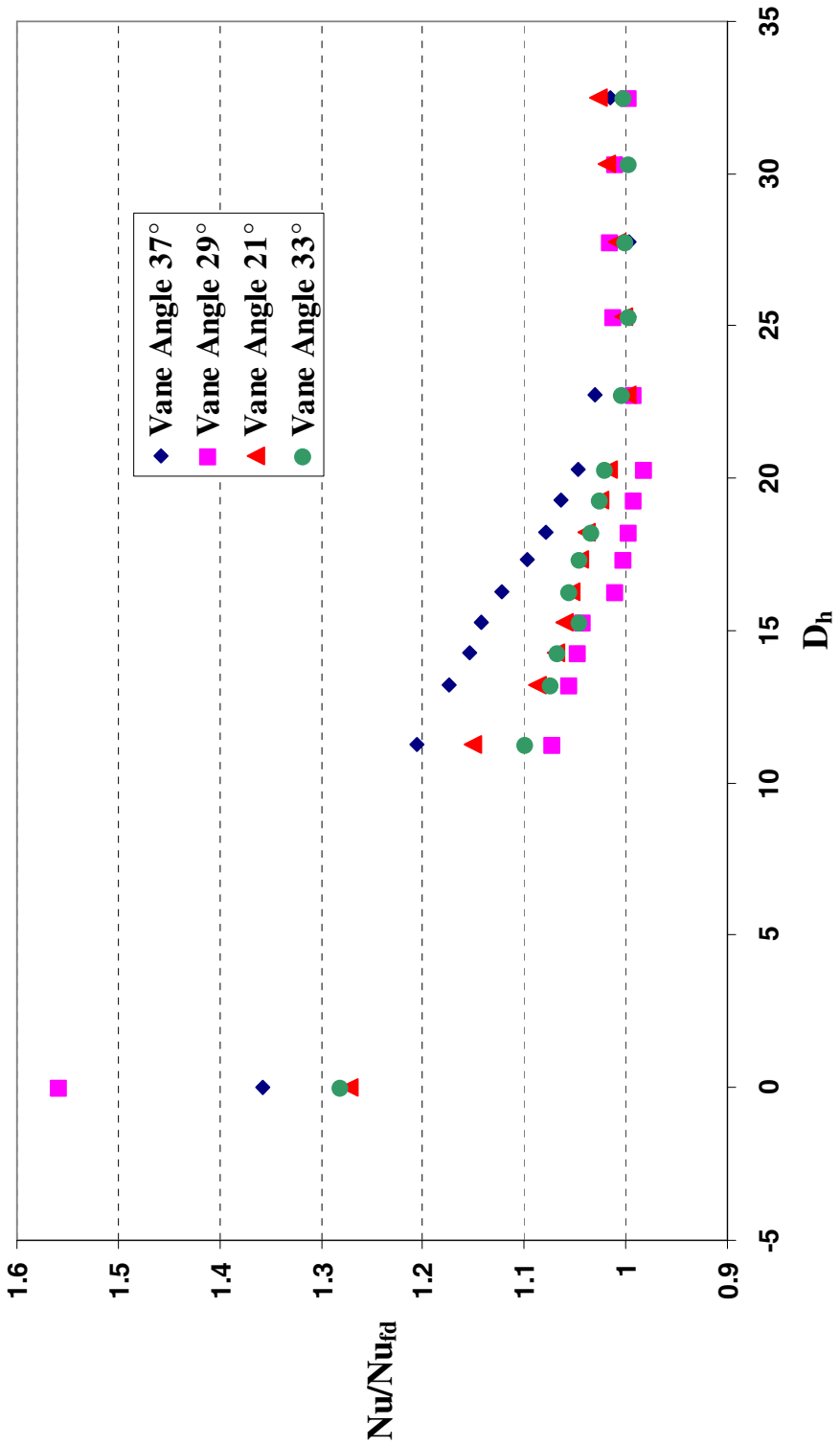

Figure A.6: Heat transfer enhancement for Vane Angles 37°, 33°, 29°, and 21°

REFERENCES

B.R. Munson, D.D. Joseph, "Viscous Incompressible Flow Between Concentric Rotating Spheres," J. Fluid Mech., vol. 49, pp. 289-303, 1971

Conner M., Smith D., Young M., "Azimuthal Heat Transfer Variations Downstream of Grids With Mixing Vanes," Proceedings of the International Meeting on LWR Fuel Performance, paper 1053, 2004

De' Crecy F., "The Effect of Grid Assembly Mixing Vanes on Critical Heat Flux Values and Azimuthal Location in Fuel Assemblies," Nuclear Engineering and Design., vol. 149 pp. 233-241, 1994

Guellouz M.S., S. Tavoularis, "The Structure of Turbulent Flow in a Rectangular Channel Containing a Cylindrical Rod- Part 1," Experimental Thermal and Fluid Science, vol. 23, pp. 59-73, 2000

Holloway M., "Fluid Dynamics and Heat Transfer of Turbulent Flow in Rod Bundle Subchannels," Clemson University Dept. of Mechanical Engineering, PHd Dissertation, 2005

Holloway M., Conover T., McClusky H., Beasley D., Conner M., "The Effect of Support Grid Design on Azimuthal Variations in Heat Transfer Coefficient for Rod Bundles," Journal of Heat Transfer, vol. 127, pp. 598-605, 2005

Holloway M., McClusky H., Beasley D., Conner M., "The Effect of Support Grid Features on Local, Single-Phase Heat Transfer Measurements in Rod Bundles," J. Heat Transfer, vol. 126, pp. 43-53, 2003

Ikeda K., Makino Y., Hoshi M., "Single Phase CFD Applicability for Estimating Fluid Hot-Spot Locations in a 5x5 Fuel Rod Bundle," Nuclear Engineering and Design, vol 236, pp. 1149-1154, 2006

Krauss T., Meyer L., "Characteristics of Turbulent Velocity and Temperature in a Wall Channel of a Heated Rod Bundle," Experimental Thermal and Fluid Science, vol. 12, pp. 78-86, 1996

Krauss T., Meyer L., "Experimental Investigation of Turbulent Transport of Momentum and Energy in a Heated Rod Bundle," Nuclear Engineering and Design, vol. 180, pp. 185—206, 1997

Marek K., Maubach K., Rehme K., "Heat Transfer and Pressure Drop Performance of Rod Bundles in Square Arrrays," Journal of Heat and Mass Transfer, vol. 16, pp. 2215-2228, 1972

McClusky H., Holloway M., Beasley D., Conner M., "Development of Swirling Flow in a Rod Bundle Subchannel," J. Fluids Eng," vol. pp. 747-755, 2002

McClusky H., Holloway M., Beasley D., Conner M., Smith D., "Mapping of the Lateral Flow Field in Typical Subchannels of a Support Grid with Vanes," J. Fluids Eng

Moller V., "On Phenomena of Turbulent Flow Through Rod Bundles," Experimental Thermal and Fluid Sciences, vol. 4, pp 25-35

Rehme K., "Pressure Drop Correlations for Fuel Element Spaces," Nuclear Technology, vol. 17, pp. 15-23, 1973

Shin S., Soon C., "Experimental Study of the Effect of Angles and Positions of Mixing Vanes on CHF in a 2 x 2 Rod Bundle with Working Fluid R-134," Korea Advanced Institute of Science and Technology., 373-1, 2005

Silin N., Luis J., Dario D., "Thermal Mixing Between Subchannels: Measurement Method and Applications," Nuclear Engineering and Design., vol. 227, pp. 51-63, 2004

Stovall T., "Effect of Vane Angle On Lateral Flow Field in Rod Bundle Subchannels," Clemson University Dept. of Mechanical Engineering, Honors Thesis, 2007

Yao K., Chung K., "Turbulent Flow Through Spacer Grids in Rod Bundles," Journal of Fluids Engineering, vol. 120, pp. 786-791, 1982